This article has been accepted for publication in a future issue of this journal, but has not been fully edited. Content may change prior to final publication. Citation information: DOI 10.1109/JIOT.2021.3128290, IEEE Internet of Things Journal

Robust Continuous Authentication Using Cardiac Biometrics from Wrist-worn Wearables

Tianming Zhao*, Yan Wang*, Jian Liu†§, Jerry Cheng‡, Yingying Chen§ and Jiadi Yu¶
*Temple University, Philadelphia, PA, USA 19122 †The University of Tennessee, Knoxville, TN, USA 37996
‡New York Institute of Technology, New York, NY, USA 10023 §Rutgers University, New Brunswick, NJ, USA 08901 ¶Shanghai Jiao Tong University, Shanghai, P.R. China 200240
Email:{tum94362,y.wang}@temple.edu, jliu@utk.edu, jcheng18@nyit.edu, yingche@scarletmail.rutgers.edu, jiadiyu@sjtu.edu.cn

***Abstract*—Traditional one-time user authentication is vulnerable to attacks when an adversary can obtain unauthorized privileges after a user's initial login. Continuous user authentication (CA) has recently shown its great potential by enabling seamless user authentication with few users' participation. We devise a low-cost system that can exploit users' pulsatile signals from photoplethysmography (PPG) sensors in commodity wearable devices to perform CA. Our system requires zero user effort and applies to practical scenarios that have non-clinical PPG measurements with human motion artifacts (MA). We explore the uniqueness of the human cardiac system and develop adaptive MA filtering methods to mitigate the impacts of transient and continuous activities from daily life. Furthermore, we identify general fiducial features and develop an adaptive classifier that can authenticate users continuously based on their cardiac characteristics with little additional training effort. Experiments with our wrist-worn PPG sensing platform on 20 participants under practical scenarios demonstrate that our system can achieve a high CA accuracy of over 90% and a low false detection rate of 4% in detecting random attacks. We show that our MA mitigation approaches can improve the CA accuracy by around 39% under both transient and continuous daily activity scenarios.**

***Index Terms*—Continuous Authentication, Wearables, Photoplethysmography (PPG), Biometrics**

I. Introduction

Traditional user authentication methods rely on users' inputs, such as passwords and graphic patterns. However, these methods are known to be vulnerable to many attacks [1], [2]. Recently, multi-factor authentication (MFA) [3], [4] has been proposed to mitigate these threats by verifying two or more confidential information from independent sources. While many applications have adopted either one-factor or MFA, both of these two approaches use a one-time login process, which is not secure enough to authenticate users in the duration of certain applications. This is especially critical for a security-sensitive application, in which an adversary could obtain unauthorized privileges after a user's initial login. Therefore, a practical continuous user authentication (CA) solution that can periodically verify a user's identity without interruptions of the application usage is highly in demand [5].

Existing CA approaches usually focus on reducing or eliminating user involvement in the authentication process by leveraging users' unique behavioral patterns. For example, keystroke/mouse dynamics [6], [7] and gait patterns [8] have been used for user authentication since 2012. These approaches usually rely on momentary events and can only determine a user's identity by monitoring particular activities (e.g., typing, mouse-clicking, or walking). Recently, researchers have also shown the potential for attacking the behavioral-based CA systems. For instance, Yu *et al.* [9] show the practicability of an indirect eavesdropping attack to infer keystrokes of touch screen leveraging audio devices on a smartphone. There are studies using cardiac signals (e.g., ECG [10], [11] and cardiac motion [12]) for CA. All these systems require dedicated sensors (e.g., ECG or Doppler radar sensors), which are costly and not readily available in commodity devices. Recently, researchers find that the photoplethysmography (PPG) sensor can also provide unique cardiac biometric information for user authentication [13]–[16]. However, these systems only focus on clinical scenarios, under which strong and stable PPG measurements are collected from the fingertips of static subjects.

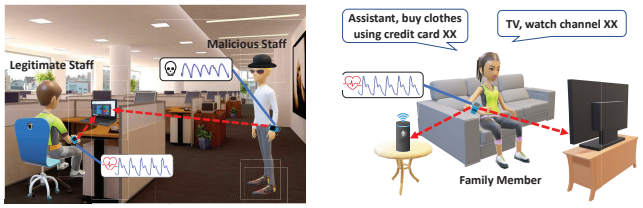

(a) CA in office scenarios (b) CA in living scenarios

Fig. 1: Two scenarios of continuous user authentication (CA) using TrueHeart.

Different from the existing works, we develop a low-cost CA system, TrueHeart, which can periodically verify the identity of a user via cardiac signals (i.e., PPG) from common wrist-worn wearable devices (e.g., smartwatches and fitness trackers). Under a working environment shown in Figure 1(a), TrueHeart can continuously determine whether a current staff operating a specific device (e.g., a smartphone or a laptop) is a legitimate user in a non-intrusive manner so that any time-sensitive tasks will not be interrupted. As a result, a user can continuously trade stocks, manage air traffic, or switch circuits. As a daily life example in Figure 1(b), each family member with a wearable device can be periodically authenticated by TrueHeart so that he/she can enjoy a seamless experience of

accessing or switching between user-specific apps on the smart devices paired with TrueHeart. Therefore, each person can watch his/her own favorite channels in a smart TV or do online shopping via a voice assistant. The advantage of using PPG for CA is obvious as cardiac signals are unique and ever-present biometrics which are available without users' involvement. In addition, PPG requires physical contact to human skin and is usually hidden in the back of wearable devices. Therefore, PPG measurements are secure and difficult to counterfeit.

There are several challenges in performing CA using PPG measurements from wearable devices. First, *in contrast to ECG signals* which is electrical and generated by heart activities, PPG signals capture blood volume changes by measuring reflected light from human skins. Therefore, PPG signals are relatively coarse-grained, noisy, and more susceptible to interference than ECG signals. Initial works have shown that PPG measurements from fingertips contain unique features to be used for user authentication in clinical environments but these features are not persistent in the PPG signals collected from wearable devices in practice. Second, wrist-worn wearable devices are usually associated with a lot of hand or body movements from daily activities. These movements would result in various motion artifacts (MAs) which make cardiac signals in PPG measurements often unavailable in practice. Third, due to various types of imprecisions in PPG sensors in wearable devices and loose contacts between them and human skins, cardiac signals from PPG measurements could vary among days or even in the same day.

To address these challenges, we particularly investigate and determine *general fiducial features* that are not only persistent in various users' PPG measurements but also can capture unique characteristics of cardiac motions for CA. Additionally, we study the MAs of different types of body-movements in practical scenarios and develop effective MA detection methods to differentiate two types of MAs: *transient MAs* and *continuous MAs* according to their occurrence frequency and durations. We categorize the transient MAs into two categories depending on whether they are caused by *far-wrist activities* or *near-wrist activities*. *Transient MA mitigation/removal mechanisms* are designed to either recover cardiac signals from weak transient MAs from *far-wrist* activities or remove the sensor measurements containing strong transient MAs from *near-wrist activities*. Moreover, a *continuous MA mitigation pipeline* is proposed to mitigate the impacts from continuous MAs effectively. We exploit advanced machine learning methods and adopt the Gradient Boost Tree (GBT) classifier to enable robust and accurate CA under practical scenarios in our daily lives. Our system also adopts an *adaptive updating mechanism* to automatically accommodate the user's cardiac signal changes over time based on an adaptive training mechanism. The main contributions of our work are summarized as follows:

- We develop TrueHeart, the first low-cost CA system that can authenticate users by using unique cardiac biometrics extracted from PPG sensors in wrist-worn wearable devices. Our system can be easily deployed in any PPG-enabled wearable device (e.g., smartwatches and activity trackers).
- We extensively study the characteristics of MAs under various practical scenarios and develop an *MA detection* method that can effectively identify different categories of MAs with various durations and intensities. A robust *transient MA mitigation/removal mechanism* and a *continuous MA mitigation pipeline* are proposed to eliminate the impacts from the *transient MAs* and *continuous MAs*, respectively.
- We identify general fiducial features that can capture the uniqueness of users' cardiac patterns to build an adaptive gradient boosting tree (GBT)-based classifier that is not susceptible to PPG signal drifts and various practical attacks during when authenticating users.
- We build a prototype of TrueHeart using both commodity PPG sensors and smartwatches. Experimental results involving 20 participants demonstrate that TrueHeart can achieve a high average CA accuracy of over 90% while maintaining a low false detection rate of 4% when detecting random attacks.

II. Related Work

Recent user authentication systems often use users' biometrics (e.g., behavioral or physiological information) to reduce user involvement and facilitate CA. Behavioral pattern is considered a distinct biometric that can make CA possible based on users' daily activities. For example, Mondol *et al.* [17] propose a user authentication system leveraging motion sensors in smartwatches to capture users' signatures in the air for authentication. Casale *et al.* [18] develop a wearable-based authentication system based on users' walk patterns. However, these approaches rely on users' involvement in specific activities in such a great deal to easily cause inconvenience.

Physiological-based biometrics (e.g., cardiac and respiratory motions) are popularly used for building CA systems because they can be obtained without users' active participation. For instance, Lin *et al.* [12] propose a CA system, Cardiac Scan, which utilizes DC-coupled continuous-wave radar to capture distinct heart motions in the user identification process. Rahman *et al.* [19] develop a method that uses the Doppler radar to identify users based on their respiratory motions. Although these systems provide a sound foundation for CA using wireless technology, they use dedicated devices that might not be available for users yet. Recently advanced sensing technologies enable unobtrusive and continuous user authentication based on unique cardiac biometrics captured by electrocardiogram (ECG) sensors [20], [21]. While mostly available under clinical environments, these systems require users to wear electrodes at various locations. This again turns out to be inconvenient for the uses in practice.

Unlike ECG, PPG is widely used in commodity wearable devices such as smartwatches and fitness trackers. Some initial studies have explored PPG-based authentications. For example, fiducial features [13], [14] have been discovered to capture unique characteristics in human cardiac systems so they can facilitate user authentication processes. Recently, non-fiducial features (i.e., discrete wavelet transform (DWT) coefficients) of PPG signals are proposed to build CA systems [15], [16]. However, all of the aforementioned studies collect PPG measurements from users' fingertips thus require users to wear dedicated PPG sensors and keep motionless. These requirements are different to meet in reality.

This article has been accepted for publication in a future issue of this journal, but has not been fully edited. Content may change prior to final publication. Citation information: DOI 10.1109/JIOT.2021.3128290, IEEE Internet of Things Journal

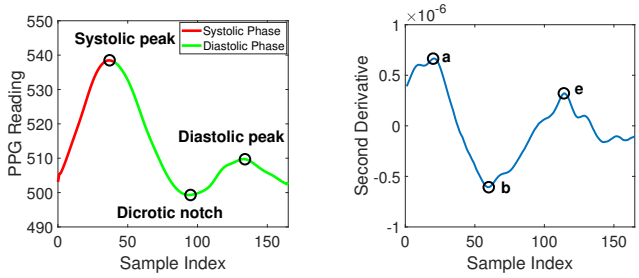

(a) Raw PPG measurements

(b) Second derivative of raw PPG measurements

Fig. 2: Illustration of the critical landmarks in raw PPG measurements and its second derivative.

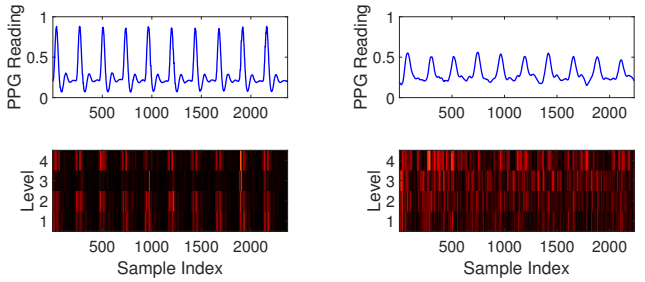

(a) Fingertip PPG data and DWT coefficients

(b) Wrist PPG data and DWT coefficients

Fig. 3: Example of PPG data from fingertip & wrist and their corresponding discrete wavelet transform.

Different from the existing work, we build the first low-cost PPG-based system that can perform CA in practical scenarios with various body movements by leveraging PPG sensors in commodity wrist-worn devices. We identify general fiducial features that can capture distinct cardiac biometrics of diverse PPG measurements collected from users' wrist areas. In addition, we extensively study the PPG MAs caused by daily activities and develop the robust methods to mitigate the impacts from transient and continuous MAs accordingly. Moreover, our system employs an adaptive user authentication method that can reduce the impact of system drifts and provide long-term PPG-based CA.

III. Approach Overview

A. Attack Model

In this paper, we assume that attackers cannot compromise users' wearable devices (i.e., gaining access to their memory storages for raw PPG measurements). Based on this, the possible attacks to our CA system are as follows:

Random attack. Attackers or their accomplices wear users' wearable devices and expect the PPG measurements captured can pass our PPG-based CA system. This random attack model is similar to the brute-force attack.

Synthesis attack. To launch this attack, attackers first need to obtain users' blood flow patterns through either medical records or vision-based technologies (e.g., remote photoplethysmography (rPPG) [22]). However, these patterns and the PPG measurements collected from users' wrist areas are different in collection approaches and conditions. In addition, the PPG signals are collected in an enclosed environment (between the back of wearable devices and skin contact areas) so that it is very hard for the attacker to obtain the user's PPG measurements. As a result, synthesis attacks will not be easily launched.

B. Feasibility Study

Intuition of Using Wearable PPG for CA. Human cardiac systems have been studied and known to be distinct among people [23]. Along this direction, initial studies [14], [24] have shown that *fiducial features* derived from critical landmarks in the raw PPG measurements and their derivatives (i.e., the systolic/diastolic peaks, dicrotic notch, and points a/b/c in Figure 2) can be used as users' unique biometric information. However, these studies only analyze PPG data collected from clinical settings with quite strict requirements. Thus, how to design and realize a PPG-based CA system using wrist-worn devices in practices remains a challenging task.

Difference between Wrist-Worn PPG and Fingertip PPG. To illustrate such a difference, we collect PPG measurements from both fingertip and wrist areas of the same users simultaneously using our prototype PPG sensing platform. The top two panels of Figure 3 show that the PPG measurements from the wrist area are stable but with less detectable and critical landmarks than those from the fingertip area. This indicates that the existing fiducial-feature-based authentication approaches [14], [24] are not applicable directly to the PPG from wearable devices. We further generate non-fiducial feature for both PPG measurements using the Daubechies wavelet of order 4 (db4) with four levels of decomposition. The bottom two panels in Figure 3 show that the fingertip PPG readings have repetitive and stable DWT coefficients with respect to each heartbeat in four levels, whereas the wrist area PPG readings are embedded with many noisy and irregular DWT coefficients, which will significantly impact the performance of the non-fiducial-based PPG authentication work [15], [16]. Therefore, instead of adopting non-fiducial features, there is a need to explore more general fiducial features in the PPG signal from the wrist area for CA, which is explained at *PPG Feature Extraction and User Authentication* in Section IV.

Impact of Daily Activities. To better understand the impact of daily activities as motion artifacts (MAs), we categorize them into two types: *transient MAs* and *continuous MAs* according to their occurrence frequency and durations. In particular, *transient MAs* refer to the motion artifacts with a very short time duration, which are generated by the transient daily activities (e.g., drinking water movements last less than 10 seconds). Depending on the distance from the location of the MA to the wrist and their impacts on PPG signal, we further define three categories for transient MAs: *far-wrist*, *near-wrist*, and *whole-body*. The far-wrist activities are the major arm movements without involving tendons and muscles of the wrist area. In contrast, the near-wrist activities are finger-level and/or wrist-level movements, which have direct impacts on blood volume changes in the wrist area and more significant impacts on PPG measurements from wearable devices. The whole-body activities are associated with most human body parts. We find that some whole-body activities of low intensity, such as leisure walking, do not have noticeable impacts on the PPG measurements. More strenuous activities, such as running,

This article has been accepted for publication in a future issue of this journal, but has not been fully edited. Content may change prior to final publication. Citation information: DOI 10.1109/JIOT.2021.3128290, IEEE Internet of Things Journal

would change PPG readings significantly. Different from the transient MAs, *continuous MAs* refer to the motion artifacts lasting for a much longer period of time, which are generated by continuous daily activities (e.g., brushing teeth lasts at least 1 minute). Continuous MAs can have different degrees of impact on PPG signals during their long-time occurrences. Such characteristics make them more challenging to tackle. In this work, we focus on the static and moving scenarios involving the transient MAs and continuous MAs, which cover the main scenarios in continuous user authentication in daily life. We present the detailed design of our system in the following sections.

C. System Overview

The architecture of our PPG-based continuous user authentication system is shown in Figure 4. The system collects PPG measurements constantly from users' wearable devices as the input. Due to hardware imperfection, the raw PPG measurements inevitably contain baseline drifts and high-frequency interferences. Therefore, our system first performs *Noise Reduction using Filtering* to reduce such impacts. A band-pass filter is used to extract pulsatile components in PPG measurements. After filtering, the system conducts *Pulse Segmentation* to determine the PPG segment that is likely to contain a complete cardiac cycle. The insight is that each cardiac cycle should include a *systolic peak*, which could be identified in the PPG measurement during typical diastole and systole phases.

Next, we design *Motion Artifact (MA) Filtering* to mitigate MAs caused by daily physical activities. In PPG measurements, MAs arise from tissue deformations and local blood flow changes in the wrist area. While pulsatile signals are repetitive in PPG measurements, most MAs have burst PPG waveforms. We calculate statistical measures, such as kurtosis, skewness, and standard deviation, in pulse waveforms and MA signals to determine whether a PPG segment contains a pulse or an MA in the *MA detection* process. If MAs are detected, our system adaptively performs two MA mitigation approaches according to the duration of the MAs. Specifically, when the detected MAs are transient and scattered, our system performs *transient MA mitigation*. Those transient MAs are either mitigated or removed based on their classified impacting sources (i.e., *far-wrist* and *near-wrist* activities), respectively. When the detected MAs last for a long time continuously, our system performs the *continuous MA mitigation* pipeline to separate the pulse waveforms from continuous MAs. After the *Motion Artifact (MA) Filtering*, the data processing of our system is separated into two phases: *Training Phase* and *Authentication Phase*.

Training Phase. In this phase, our system performs *General Fiducial Feature Extraction* to extract the unique cardiac features from the PPG segment and its second derivative. This process applies to both wrist PPG measurements and fingertip ones. Next, we perform *Binary Gradient Boosting Classifier Construction* to train a binary classifier for each user. In particular, we construct a user's profile based on some extracted features and use the Gradient Boosting Tree (GBT) in training the classifier when the user enrolls in the system.

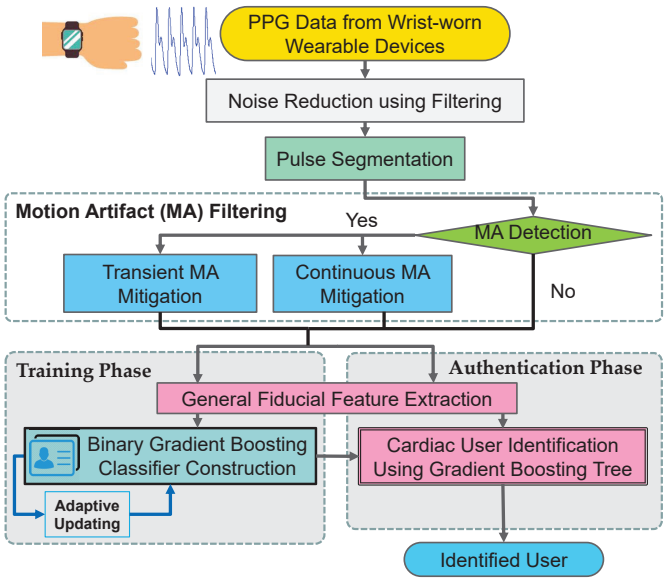

Fig. 4: Architecture of TrueHeart.

Furthermore, our system regularly updates the classifier with new training data to accommodate PPG drifts over time in *Adaptive Updating*.

Authentication Phase. In the *Authentication Phase*, our system collects PPG segments in real-time and determines whether a current user is legitimate based on the PPG segments in a sliding window. Specifically, after our system filters MAs out from the PPG segments, it would further extract general fiducial features. Then our system performs *Cardiac User Identification Using Gradient Boosting Tree* by using the binary gradient boosting classifiers generated in the training phase to determine the user's identity based on each PPG segment. Finally, our system utilizes a majority-vote rule on the classified results of the PPG segments in the sliding-window to perform CA. In addition, our CA system is suitable for commodity wearable devices since their PPG sensors consume low power (e.g. 4mA) compared to battery capacities of these devices.

D. Challenges

Accurate Sensing Using Low-cost PPG Sensor on the Wrist. The low-cost PPG sensors in commodity wearable devices collect data from users' wrists at lower sampling rates with more noise and lower resolution. This will reduce the accuracy in user authentication.

Robust CA with Body Movements in Daily Activities. The PPG sensors in the wrist-worn wearable device are particularly susceptible to daily physical activities. Daily activities involving different movements can generate the MAs with various durations and degrees of impacts on PPG signals. Especially, compared to the MAs with short durations (i.e., transient MAs), handling MAs with long durations (i.e., continuous MAs) is more challenging due to their continuity and diverse impacts. Therefore, we need to explore the characteristics of various MAs from the PPG measurements and develop technologies to adaptively reduce such impacts.

Effective Feature Set for General PPG Measurements. The PPG measurements from the wrist area are unstable and

This article has been accepted for publication in a future issue of this journal, but has not been fully edited. Content may change prior to final publication. Citation information: DOI 10.1109/JIOT.2021.3128290, IEEE Internet of Things Journal

weak, leading to fewer detectable fiducial features. Thus, we need to exam general effective features for CA.

Persistent User Authentication Against PPG Drifts. The typical system-drifts in PPG sensors which could significantly impact the CA performance. Our system should study these drifts and adaptively accommodate the resulting PPG variations during a long time period.

IV. PPG Feature Extraction and User Authentication

In this section, we explore the cardiac features extracted from PPG measurements and present the details of our adaptive user authentication method.

A. General Wrist PPG Feature Extraction

We have shown that the PPG measurements from the wrist area have fewer fiducial features and non-fiducial features compared to the PPG measurements from the fingertip. Therefore, we explore the fiducial features that are still available in the PPG measurements from the wrist area based on the 29 fiducial features that have been used for user authentication [24], [25].

General Wrist PPG Fiducial Features. Based on our experiments with 20 participants, we find that 60% of the PPG measurements from the wrist area have only one obvious systolic peak in a cardiac cycle. To let our CA system generally work for various types of PPG measurements, we select to use five fiducial features that only require a single systolic peak in the PPG measurements. The five fiducial features are generally effective for the user authentication because they are always available regardless of the source of the PPG measurements (i.e., from the wrist area or the fingertip), and they have the physiological relationships with human cardiac systems. We summarize the five fiducial features and their physiological meanings as shown in Table I. Note that the five general fiducial features are always available in the PPG measurements from the fingertip. Therefore, our CA system is also applicable to the clinical PPG measurements. We provide a detailed evaluation of our system on both our PPG data from the wrist area and the fingertip in Section VII.

TABLE I: List of General Wrist PPG Features.

Feature Name	Feature Description
Systolic Amplitude (A_s)	Related to the stroke volume and directly proportional to vascular distensibility, which is distinguishable among different people.
Pulse Width (P_w)	The width of the PPG signal at the half-height of the systolic peak, and it correlates with the systemic vascular resistance.
Ratio of Pulse Interval to Systolic amplitude (P_i/A_s)	Reflects the functionality of a person's cardiovascular system.
Crest Time (T_c)	Indicates the pulse wave velocity, which is distinct from person to person.
Ratio of Amplitude of b-wave and a-wave (A_{b-w}/A_{a-w})	Reflects the arterial stiffness and the distensibility of the peripheral artery, which are also different among people. In addition, this feature can also reflect the healthy level of different people.

B. Adaptive cardiac authentication using Gradient Boosting Tree

Next, we build the binary classifier using Gradient Boost Tree (GBT) for user authentication. Comparing to other machine learning methods, GBT can handle the mixed types of the features with different scales, which is exactly what our general fiducial feature set possesses. Moreover, GBT is robust against the outliers via the robust loss functions and can eliminate the requirement of normalizing or whitening the feature data before classification [26].

Specifically, given N training samples $\{(x_i, y_i)\}$, where x_i and y_i represent the cardiac-related feature set and the corresponding identity label of the user (i.e., y_i = 1 or -1 represents whether x_i is from the current legitimate user), GBT seeks a function $\phi(x_i) = \sum_{m=1}^{M} \omega_m h_m(x_i)$ to iteratively select weak learners $h_m(\cdot)$ and their weights ω_j to minimize a loss function as follows:

$$\mathbf{L} = \sum_{i=1}^{N} L(y_i, \phi x_i). \tag{1}$$

We specifically adopt the GBT implementation from the SQBlib library [27] for cardiac-related feature training. In order to optimize the speed and accuracy of the GBT model, we empirically choose the exponential loss $L = e^{y_i \phi(x_i)}$ as the loss function $L(\cdot)$ with enough shrinkage (i.e., 0.1) and number of iterations (i.e., $M = 2000$), and we take a fraction of 0.5 as the sub-sampling of the training dataset. Once we have determined the loss function, next we will construct a binary gradient classifier $b_k(\cdots)$ for each user $g_k, k = 1, \cdots, K$ to complete the *Training Phase*. Then for the testing feature set, each binary gradient classifier will output a score. The reason to use binary classifier is that binary classifier has higher accuracy in differentiating one user from other users [28] which exactly meets the fundamental requirement of a CA system.

In the *authentication phase*, our system utilizes the already built binary classifiers for all the users in parallel to classify incoming cardiac-related feature set x. In particular, we will obtain different confidence scores from each binary classifier, and choose the identity k of the binary classifier $b_k(x)$ with the highest score as the final classification. After the user classification, we adopt a non-overlapped sliding window-based approach to perform CA. In particular, we consider P continuous PPG segments in a sliding window as a basic CA unit and use the majority vote from the classification results of these PPG segments to determine the user's identity periodically. If equal or more than half of the PPG segments in the window are classified to be the same user, the system would allow the current user to pass the user authentication. Otherwise, the current user does not pass the user authentication. Unless mentioned elsewhere, we set the sliding window size to 4 PPG segments, which generally provides good performance as shown in our evaluation.

Adaptive Updating. We find that people's pulse patterns may slightly vary during the day. Therefore, we design our system to re-train the underlying classifier based on the recently collected PPG measurements after each successful user authentication. Specifically, our system regularly adds a small amount of the user's PPG measurements (e.g., 2min) to the training data to re-train a new classifier for the user in the

This article has been accepted for publication in a future issue of this journal, but has not been fully edited. Content may change prior to final publication. Citation information: DOI 10.1109/JIOT.2021.3128290, IEEE Internet of Things Journal

background. This re-training process will stop until the new classifier meets the performance requirement (e.g., when the CA accuracy reaches 90%), and the new classifier will take effect until the next time re-training process starts.

V. Motion Artifacts Detection and Filtering

In this section, we present the MA detection algorithm and mitigation methods for transient and continuous MAs.

A. Motion Artifacts Detection

After the pulse segmentation mentioned in Section VI, the system first needs to detect whether MA is affecting the PPG segments or not. We find that when there is no MA, the PPG segments should contain similar pulse waveform, thus the statistics of each PPG segment should be stable over time. However, when the PPG segments are affected by MA, the statistics of PPG measurements vary a lot. Therefore, we propose to examine the statistics of each PPG segment and use a threshold-based approach to detect the existence of MA.

Particularly, we choose three types of statistics (i.e., kurtosis, skewness, and standard deviation (STD)) efficiently measuring the symmetry, tails, and dispersion of the PPG segments respectively, which are used to effectively detect MA in existing work [29]. For each type of statistics, we derive its cumulative distribution function (CDF) based on high-quality PPG segments (about 20 seconds) without MA. From the CDF, we determine two thresholds that can include 95% of the values of particular statistics. The statistics of the testing PPG segments will be compared to the thresholds, respectively. If any of the three types of statistics from a PPG segment is out of the range determined by the corresponding two thresholds, the PPG segment is determined to be affected by MA. An example of the MA detection has been shown in our conference paper [30]. We note that the accuracy of our MA detection method is over 95% based on the data collected from a user's wrist in the moving-scenario described in Section VII.

In addition, considering the impacts of transient MAs and continuous MAs are different, we developed a MA classification method to differentiate these two types of MAs based on the duration of each detected MA. From our experimental results of all 20 participants, we find that most transient body or hand movements in our daily lives last less than 10s, so we define any MAs that last longer than 10s are continuous MAs. We examine the incoming PPG signals using a sliding window $\mathcal{W}$ of 10s. If all the signals within the window are determined to contain MA, the system considers these MAs are *continuous MAs*. Otherwise, the system considers them as *transient MAs*.

B. Transient Motion Artifacts Mitigation

Once the system detects transient MAs, it needs to determine whether they are caused by far-wrist or near wrist activities. We find that the far-wrist activities (e.g., moving the forearm to reach a cup) usually create sparse and mild MAs to PPG measurements, while the near-wrist activities (e.g., grabbing a cup) result in much stronger MAs for a longer period within a sliding window. Based on this observation, we develop a transient MA classification method, which examines the proportion of the PPG segments affected by MAs in a sliding window and determines whether the cause of transient MAs is the near-wrist activities or far-wrist activities using a threshold-based approach. Specifically, we define every cardiac cycle (about 1s) of PPG signal as a PPG segment. We denote the number of PPG segments determined to be affected and not affected by MA in the sliding window as M_W and N_W, respectively. Next, the system calculates the proportion of the PPG segments affected by MA in the sliding window defined as $\lambda = \frac{M_W}{N_W}$ and compares it with a threshold θ_{ma}. The detected MAs are classified as near-wrist MAs if $\lambda \geq \theta_{\mathrm{ma}}$. Otherwise, they are classified as far-wrist MAs. We find that the threshold $\theta_{\mathrm{ma}} = 30\%$ is general enough to provide the high accuracy of categorizing the transient MAs among all participants.

Transient Motion Artifacts Mitigation for Far-wrist Activities. When the system determines that the PPG segments are affected by the far-wrist activities, we notice that the interference of MA is usually small and recoverable. Therefore, we employ a special moving average filter (SMAF) to mitigate those MA and retain them for continuous user authentication. The basic idea is to average each recognized MA with several pure pulse segments (i.e., the typical PPG segments without MA) of the current testing user. Then the MA is able to be mitigated from the averaged results. Specifically, we first align the pure pulse PPG segments using the systolic peaks in order to maintain the locations of the critical fiducial points. Since the number of the samples in each pulse segment is not equal, we then interpolate those PPG segments to make them have the same length. After the interpolation, we will apply the SMAF on the pure pulse segments and MA using the following equation:

$$\mathbf{S} = \frac{\sum_{h=1}^{N} \overrightarrow{P_h} + \overrightarrow{M}}{N+1}, \tag{2}$$

where the $\overrightarrow{P_h}$ represents the pure pulse segments, $\overrightarrow{M}$ is MA that requires the mitigation, and totally N pure pulse segments and 1 MA are averaged with the mitigated result as $\mathbf{S}$. In particular, we use 4 pure pulse segments for the proposed SMAF. After the SMAF, we use the smooth function to ensure the continuity of the filtered signal. An example of the transient MA mitigation method is illustrated in our conference paper [30].

Transient Motion Artifacts Removal for Near-wrist Activities. When the system determines that the PPG segments are affected by the near-wrist activities, it implies that the PPG measurements are significantly distorted by the MA during the time in the sliding window. In this case, we remove all the PPG segments affected by MA and only perform user authentication using the rest of the PPG segments in the sliding window. However, we find that the PPG segments affected by MA may not be continuous, and the interval between two affected segments may be too short (e.g., $1 \sim 2$ seconds including $1 \sim 3$ PPG segments) for extracting a complete pulse waveform that can be used to perform user authentication. Hence, we remove all the PPG segments in between the first and last segments affected by MA and keep the unaffected

This article has been accepted for publication in a future issue of this journal, but has not been fully edited. Content may change prior to final publication. Citation information: DOI 10.1109/JIOT.2021.3128290, IEEE Internet of Things Journal

PPG segments for user authentication [30]. In addition, it should be noted that our CA system could still authenticate the user when the hand is stable before/after the near-wrist activities, and removing the transient MA caused by the near-wrist activities does not influence the user experience since user authentication can be done before the near-wrist activities.

C. Continuous Motion Artifacts Mitigation Pipeline

The aforementioned MA removal and mitigation methods are mainly designed to ensure the robustness of our system when there are transient MAs. When MAs continuously occur for a long time and are determined as *continuous MAs*, simply removing them will suspend our CA system for a long time, which significantly impacts user experience. Therefore, a continuous MA mitigation method is demanded in such scenarios. Existing work [31] has shown that the frequency range of the continuous motion artifacts is 0 to 20Hz. Since it overlaps with typical human heartbeat frequency (i.e., 0.6 to 2 Hz), traditional filtering technology cannot effectively extract cardiac signals with such motion artifacts. We design a two-phase continuous MA mitigation pipeline as shown in Figure 5. Particularly, the first phase performs *Non-heartbeat-frequency MA Mitigation* to mitigate the MAs residing out of the typical heartbeat frequency range. Then, the second phase performs *Heartbeat-frequency MA Mitigation* to mitigate the remaining MAs residing inside the typical heartbeat frequency range.

1) Non-heartbeat-frequency MA Mitigation: At first glance, Fourier transform or wavelet transform can be adopted to mitigate the MAs with non-heartbeat frequency. However, neither of these two approaches using linear decompositions [32], [33] can perform well when processing nonlinear and nonstationary PPG signals (with or without MAs).

We find that, different from Fourier transform or wavelet transform, *Variational Mode Decomposition (VMD)* and *Empirical Mode Decomposition (EMD)* are designed to decompose nonstationary and nonlinear signals by unraveling their hidden quasi-periodicity and features. Therefore, they are more suitable for analyzing nonlinear and nonstationary signals [34]–[36], such as PPG signals. In this work, we develop two approaches to mitigate the non-heartbeat-frequency MAs using VMD and EMD, respectively. The basic idea is to decompose PPG signals into a series of periodic oscillatory components with different frequencies and amplitudes. Retaining the components with frequency residing in the typical heartbeat can mitigate the non-heartbeat-frequency MA. We note these two methods are developed for different purposes. The concurrency processing of the VMD-based method enables faster MA mitigation on resource-constraint mobile devices (e.g., smartwatch and IoT devices). While EMD-based methods can achieve the competitive performance and automatically determine the optimal number of components to decompose. However, the recursive decomposition process of the EMD-based methods leads to a much larger computational cost than VMD, which makes them more suitable for the devices with more computing power (e.g., smartphone and personal computer).

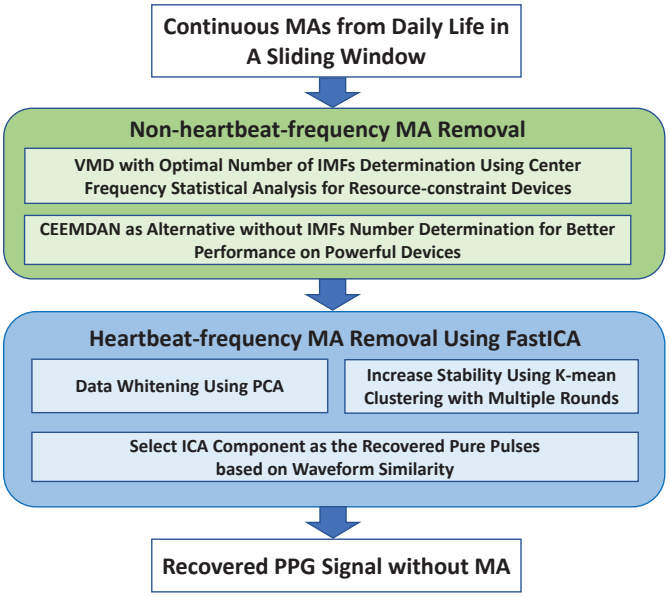

Fig. 5: Illustration of our two-phase continuous MA mitigation approach using VMD or CEEMDAN with FastICA.

The VMD-based MA mitigation method decomposes the PPG MAs in a sliding window (e.g., 12 seconds) into multiple Intrinsic Mode Functions (IMFs) that can capture the periodically oscillatory components with different frequencies. Since typical pure heartbeat PPG signals are periodic with a certain frequency range (i.e., 0.6 to 2 Hz), we only retain the VMD-decomposed IMFs corresponding to heartbeat frequency and mitigate the signal components with non-heartbeat frequencies. It should be noted that an insufficient number of IMFs cannot guarantee enough decomposition to extract all heartbeat frequency components from PPG signals. Moreover, too many IMFs overdecompose the PPG signals to introduce noises (e.g., redundant components), which have shape and frequency contents that are nonexistent in PPG signals. To ensure that the VMD-based MA mitigation can accurately extract heartbeat signals, it is important to accurately determine the optimal number of IMFs for PPG signals.Towards this end, we adopt the Center Frequency Statistical Analysis (CFSA) [37] to automatically determine the optimal number of IMFs. The main idea of CFSA is to iteratively increase the number of IMFs for decomposition until the number of IMFs that have their center frequencies higher than the average center frequency of all the IMFs no longer increases. The initial number of IMFs in VMD is empirically set to 4 based on our experiments to reduce the iterations to find the optimal number of IMFs.

The EMD-based method basically decomposes the PPG signals using a different theoretical framework. In particular, we adopt the Complete Ensemble Empirical Mode Decomposition with Adaptive Noise (CEEMDAN) [38] to avoid the mode mixing problem in traditional EMD and provide better mode separation. Different from VMD, CEEMDAN works as a self-adaptive filter that can automatically determine the optimal number of IMFs for the decomposition. Therefore, we can apply CEEMDAN to decompose the PPG MAs in a sliding window (e.g., 12 seconds) without specifying the

This article has been accepted for publication in a future issue of this journal, but has not been fully edited. Content may change prior to final publication. Citation information: DOI 10.1109/JIOT.2021.3128290, IEEE Internet of Things Journal

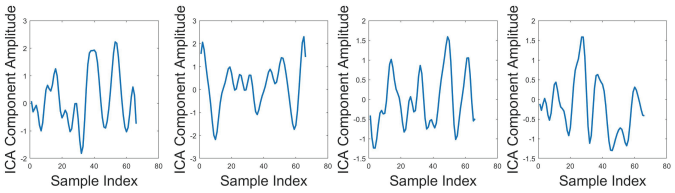

Fig. 6: The cluster centroids of 4 ICA components (i.e., *Comp1*, *Comp2*, *Comp3*, and *Comp4*) with applying our FastICA pipeline on the remaining MAs (e.g., generated by washing dishes) after non-heartbeat-frequency MA mitigation.

number of IMFs. Then, we retain the CEEMDAN-decomposed IMFs in the typical heartbeat frequency range to mitigate the non-heartbeat-frequency MAs. The key to having a decent performance of CEEMDAN is properly setting its two main parameters (i.e., the added noise on MAs and the number of ensemble trials). Particularly, the white noise with an appropriate amplitude is required to solve the mode mixing problem and avoid the redundant IMFs. Moreover, a sufficient number of ensemble trials is theoretically needed to remove the effect of the added noise. We find that CEEMDAN provides the best decomposition performance for the PPG MAs when the amplitude coefficient is 0.2 and the number of the ensemble trials is 500.

Based on our experiments, we observe that CEEMDAN can decompose more low frequency components below 0.6 Hz which makes it more effective than VMD for correcting the low-frequency motion artifacts in daily life. We note that both continuous MA mitigation methods process PPG data in a sliding window. We empirically determine the size of the window to be 12s, which covers sufficient extreme of the signals for both methods to work properly. After decomposing the MAs by either of the methods, we only retain the IMFs with the frequency residing in the ranges of typical heartbeat (i.e., 0.6 to 2 Hz).

2) Heartbeat-frequency MA Mitigation Using ICA: After non-heartbeat-frequency MA mitigation, we need to further remove the remaining MAs with heartbeat frequency. Given the fact that the pure pulse signals embedded in the remaining MAs are relatively stable and periodic, the remaining MAs are mixed independent sources that are composed of the pure pulse signals and the motion related signals. Independent Component Analysis (ICA) is a blind source separation technique used to find the independent source signals even when they have the same frequency range. Therefore, ICA can be adopted to separate the pure pulse signal out of the remaining MAs. In particular, FastICA [39] is used in our work since it is computationally efficient and has faster convergence than the conventional ICA.

A major problem of ICA algorithm is that the reliability of the estimated independent components is not known. Specifically, ICA algorithm generates different components when running multiple times. One reason is the algorithm only finds a local minimum of the objective and many local minima can be equally good. The other reason is the finite sample size inevitably induces statistical errors in the estimation. In order to deal with this reliability issue of ICA, we propose a pipeline to extract the stable source signals. We first adopt Principal Component Analysis (PCA) to whiten the input data which is necessary for FastICA to work properly. Specifically, we only retain the most uncorrelated variables based on an empirical threshold on their eigenvalues. To extract the reliable independent components, we run FastICA multiple times and obtain a set of components. If an independent component is reliable, every run of the algorithm should produce the components that are very close to the ideal components corresponding to the cluster centers. And we adopt a K-mean clustering approach to extract the stable source signals (i.e., the recovered pulses and motion artifacts). The details of the proposed pipeline are as follows:

TABLE II: Find ICA Component as the Recovered Pure Pulses according to Signals' Waveform, Periodicity, and Dominant Frequency

	Comp1	Comp2	Comp3	Comp4
DTW Distance	29	37	**24**	31
Sum of Absolute Autocorrelation Coefficients	9.4	12.1	**12.4**	8.2
Dominant Frequency (Hz) using FFT	1.5	0.9	**1.2**	1.8

- **Data Preparation and Whitening.** The remaining MAs in a sliding window is equally divided into N segments (e.g., 4) to generate sufficient dimensions of input data for FastICA. The input data is then preprocessed using PCA. Based on our experiment, we empirically keep the PCA components whose eigenvalues sum exceeds the threshold (i.e., 80%) of the sum of all the components' eigenvalues.
- **FastICA with Multiple Runs.** The FastICA algorithm runs *M* times. In our work, we set running time *M* to 10 which is sufficient to get reliable components based on our experiments. And we find the following FastICA parameters provide the best separation performance: the decorrelation approach is symmetric which speeds up the algorithm using parallelism, and the nonlinearity used is 'skew' ($g(u) = u^2$).
- **ICA Components Clustering.** The k-mean clustering approach is then adopted to cluster all the estimated independent components from the previous step according to the Euclidean distance among them. Particularly, we use the centroid of each cluster as the finalized stable components for further analysis.

For example, our proposed pipeline generates 4 clusters of ICA components from the results of 10 times of running FastICA algorithm for a washing dishes activity that lasts 25 seconds. As shown in Figure 6, we adopt the centroid of each cluster as the finalized stable ICA components from which we will find one as the recovered pure pulses.

We next find the ICA component as the recovered pure pulses, the basic idea is to select an ICA component as similar as possible to the pure pulses in terms of the waveform shape. Our selection strategy is to first find the ICA component with the smallest dynamic time warping (DTW) [40] distance to a typical user's static pulse signals of the same time duration. To guarantee the robustness of the selection, its periodicity and dominant frequency should be further considered. Based on our experiments, the correctly selected ICA component should also be the most periodic one which has the largest sum of absolute autocorrelation coefficients. Moreover, its dominant frequency from FFT must reside in the typical frequency range of the human heartbeat. With meeting all those conditions, then

This article has been accepted for publication in a future issue of this journal, but has not been fully edited. Content may change prior to final publication. Citation information: DOI 10.1109/JIOT.2021.3128290, IEEE Internet of Things Journal

we will use this ICA component as the recovered pure pulses. Otherwise, we do not adopt any ICA components from the current sliding window.

For instance, we calculate the DTW distance, the sum of absolute autocorrelation, and dominant frequency of 4 ICA components (i.e., *Comp1* , *Comp2*, *Comp3*, and *Comp4*) in Figure 6, respectively. Their detailed results are shown in Table II. We can find that Comp3 is first selected since it has the smallest DTW distance (i.e., 24) among 4 components. Since it also has the largest sum of absolute autocorrelation coefficients as 12.4 with a reasonable 1.2 Hz dominant frequency. Therefore, we select Comp3 as the recovered pure pulses based on our selection strategy. Besides, since FastICA generates normalized components [41], the selected ICA component cannot retain the original amplitude. Therefore, we scale its amplitude back according to the typical scale on the static pure pulse period. Specifically, we first apply the FastICA on the static pure pulse period (e.g., 1 min) and calculate the scales for recovering each segment. Then, the median scale value is adopted to scale the recovered MAs amplitude back.

It should be noted that the sliding window length is not fixed in our work. Since the signal length theoretically impacts the performance of VMD, CEEMDAN, and FastICA, there exist some constraints for the window length selection. Specifically, a sliding window should be long enough to capture sufficient extreme of the signals for VMD and CEEMDAN to work properly. Based on our experiment, the length of sliding window should be at least 10 seconds. Considering our basic authentication unit (e.g., 3 seconds), a 12 seconds sliding window (i.e., 4 authentication units) is adopted as the shortest acceptable window length in our work. In fact, a properly longer sliding window enables a finer-grained VMD and CEEMDAN decomposition and also leads to better source separation in FastICA. However, too long window length could generate "false" components to IMFs and increase the running time significantly [42]. Therefore, there is also a maximum length constraint. According to our experiment, a sliding window of 24 seconds at maximum could not only lead to an optimal mitigation performance but also with an acceptable running time (less than 3 seconds) for quick authentication response.

VI. PPG Data Preprocessing and Segmentation

A. Data Preprocess

The PPG measurements from the low-cost PPG sensor in wrist-worn wearable devices inevitably contain baseline drift and high-frequency interference. Since the frequency of the pulsatile component in PPG is $0.5-4$Hz, and the frequency of MA is 0.1Hz and above, our system firstly applies a bandpass filter to reduce the effect of the baseline drift and high-frequency noise. In particular, we implement a Butterworth bandpass filter with the passband $0.5-6$Hz and the order as 2 to only retain the pulsatile components together with the MA components having a similar spectrum.

B. Pulse Segmentation

Our system determines the starting and ending points of all the PPG segments in the sliding window. Ideally, we can find all the valley points in the sliding window and extract the data between every two valley points as the PPG segments. However, we find that the dicrotic notch could have the lowest amplitude (i.e., "fake" valley) in the cardiac cycle. Particularly, we tackle this issue based on the fact that the time distances from the systolic peak to the starting and ending points are in the range of $T_s = 0.15\text{s}\sim 0.26\text{s}$ and $T_e = 0.44\text{s}\sim 0.74\text{s}$, respectively [43]. Therefore, the accurate PPG segment can be extracted by selecting the valleys that are within the typical time ranges T_s and T_e before and after each systolic peak, respectively. In addition, through our experiments with 20 participants, we empirically determine the sliding window as 2s larger than one typical pulse waveform (e.g., $0.6 \sim 1$ second) to ensure the effectiveness and accuracy of the PPG segmentation. We also note that our segmentation method is effective with MA because the system finds PPG segments in the sliding window based on the peaks and valleys that fulfill the criteria even though the waveform may be distorted.

Fig. 7: Prototype: wrist-worn PPG sensing platform.

VII. Performance Evaluation

A. Experimental Methodology

Wearable Prototype. We design a wrist-worn PPG sensing prototype as shown in Figure 7, which refers to the layout of PPG and motion sensors in commodity wrist-worn wearable device (e.g., Apple Watch). Specifically, the prototype consists of one commodity green LED PPG sensor attached to the inner side of the wristband and a motion sensor (i.e., accelerometer) attached to the outside of the wristband. These sensors are connected to an Arduino UNO (REV3) board for the sensor measurements acquisition, which is under a $300Hz$ sampling rate. The PPG measurements are transferred to a laptop (i.e., Dell Latitude E6430) to perform user authentication.

Smartwatch Prototype. We have also implemented our CA system on the commodity smartwatch shown in Figure 8 to demonstrate the practical usability of our system. This prototype is composed of a smartwatch for collecting the real-time PPG measurements, a laptop running the WebSocket server to receive the data and perform continuous user authentication, and a WLAN enabling the communication between the smartwatch and the laptop via a WiFi access point. Before our CA system begins, the smartwatch and the laptop need to connect to the WLAN. Then our developed web application as the WebSocket client running on the smartwatch can initiate the connection to the WebSocket server running on the laptop. Once the connection is built, the smartwatch will transfer the real-time PPG measurements to the connected laptop via WLAN. Simultaneously, the laptop will process the incoming real-time PPG measurements and perform our CA system implemented using Matlab. In particular, we do the experiment

This article has been accepted for publication in a future issue of this journal, but has not been fully edited. Content may change prior to final publication. Citation information: DOI 10.1109/JIOT.2021.3128290, IEEE Internet of Things Journal

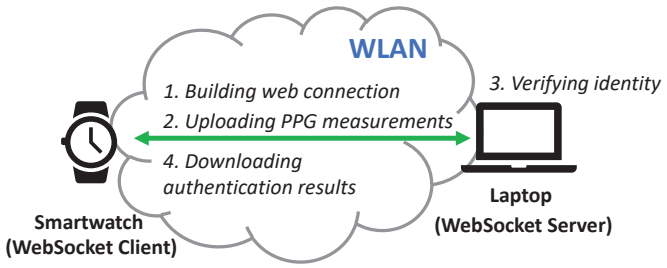

Fig. 8: Prototype using the commodity smartwatch.

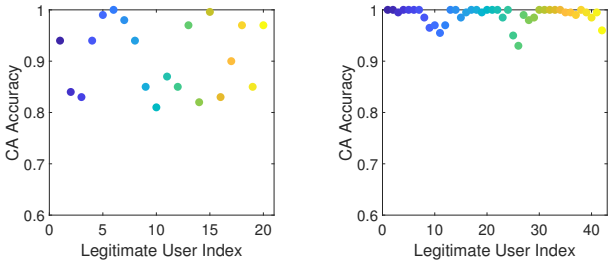

(a) PPG from the wrist area (b) PPG from the fingertip

Fig. 9: CA accuracy of TrueHeart using the PPG measurements from the wrist areas and the fingertips.

using a Samsung Gear S3 classic smartwatch with Tizen OS 4.0 which is equipped with two PPG sensors having a sampling rate of 20 Hz. The laptop is with Intel(R) Core(TM) i7-9750H CPU and 32 GB of RAM.

Data Collection. We recruit 20 healthy participants whose ages are between 20 to 40 to collect PPG measurements using our wearable prototype. Two different scenarios are adopted to evaluate our system for various practical application scenarios: In the *static scenario*, 20 participants are asked to sit quietly for 10 mins, respectively. While in the *moving scenario*, we ask 5 participants to perform the *far-wrist activities* (i.e., moving the forearms) and the *near-wrist activities* (i.e., grabbing up a cup and drinking water) repeatedly for 2 mins and sit still for 3 mins. In total, we collect around $15,000$ PPG pulse segments from the wearable prototype in the static-scenario and $4,200$ pulse segments in the moving-scenario, respectively. In addition, we also test our system on the IEEE TBME Benchmark dataset [44], which has 8-mins PPG data collected from the fingertips of 42 people with a sampling rate of 300 Hz.

For the experiments involving continuous motion artifacts, we collect PPG measurements using our smartwatch prototype. Particularly, we ask 4 participants to perform 7 continuous movements repeatedly for 2 mins and hold still for 3 mins. Those movements include different forearm and whole arm movements with various motion patterns (e.g., *forearm forward-backwards*, *forearm left-right*, *forearm half-cycle*, *whole arm left-right*, *washing dishes*, *washing face*, and *brushing teeth*). In total, we collect around 5300 PPG pulse segments in the static and 3100 pulse segments in the continuous movement, respectively.

B. Evaluation Metrics

Our system periodically authenticate the user based on the PPG segments in a sliding window and labels the sliding window as the user or attacker, respectively. We define our evaluation metrics as follows:

CA Accuracy. The number of sliding windows that are correctly labeled as the user over the total number of sliding windows that are examined during the CA process.

Attack Detection Rate. The number of sliding windows that are correctly labeled as the attacker over the number of sliding windows that are associated with the attacker during the CA process.

Attack False Detection Rate. The number of sliding windows that are incorrectly identified as the attacker over the number of sliding windows that are associated with the user during the CA process.

Receiver Operating Characteristic (ROC) Curve. It reflects the trade-off between Attack Detection Rate and Attack False Detection Rate. The smallest distance from the point on the ROC curve to the top-left corner corresponds to the optimum model.

In our evaluation, 20 rounds of Monte Carlo cross-validation are employed for the 10-mins of the collected user data, among which 5-mins for training and the rest of the data for authentication.

C. Continuous Authentication (CA) Performance

We first evaluate the general performance of TrueHeart by examining the CA accuracy in the static scenario. In particular, we consider each participant acts as a legitimate user once while remaining participants act as attackers. Figure 9(a) shows that each user achieves comparable high CA accuracy with an average of 90.73% CA accuracy, which indicates that TrueHeart can successfully authenticate users with high accuracy using the wrist-worn wearable devices. In addition, Figure 9(b) shows that our system can achieve even better performance on the PPG data from the fingertip [44] with 39 out of 42 people having the CA accuracy above 96%. This is because the PPG measurements from the fingertip are stronger and stabler than the wrist area. These results not only demonstrate the promising practical usability of our proposed user authentication system on common wrist-worn wearable devices but also indicate that it has promising usage in clinical environments such as telemedicine and smart-health applications.

Moreover, to study the performance of our system when defending against the random attack, Figure 10 shows that the ROC curve gets closer to the point $(0, 1)$ when the number of the PPG segments in a sliding window becomes larger. Particularly, our attack detection rate reaches to over 88% with the attack false detection rate of around 3.9% when the length of the sliding window is 4. And our system can achieve over 90% attack detection rate and less than 4.2% attack false detection rate with six or more PPG segments in a sliding window. Those results show that our CA system is robust against the random attacks.

D. Impact of Various Factors

Impact of the Sliding Window Length. The length of the sliding window corresponds to the number of continuous PPG segments to perform the majority vote for user authentication.

This article has been accepted for publication in a future issue of this journal, but has not been fully edited. Content may change prior to final publication. Citation information: DOI 10.1109/JIOT.2021.3128290, IEEE Internet of Things Journal

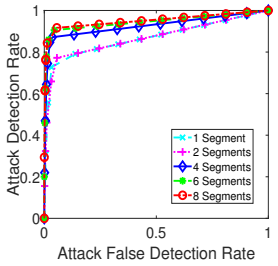

Fig. 10: ROC curves under the random attack.

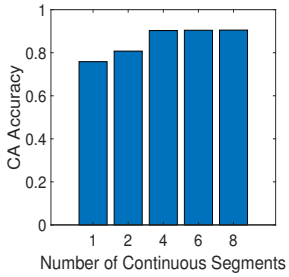

Fig. 11: Performance with different lengths of the sliding window.

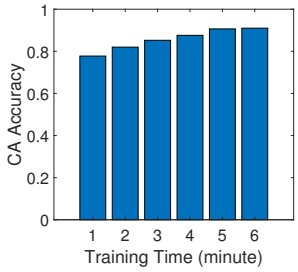

(a) Performance with different sizes of the training data

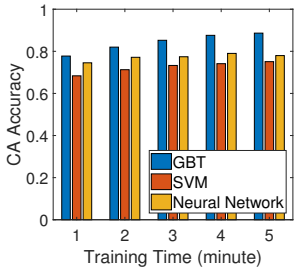

(b) Performance with different machine learning methods

Fig. 12: The impacts of the training size and the machine learning method.

Particularly, we test the different lengths of the sliding window with 1, 2, 4, 6, 8 continuous PPG segments (i.e., about 0.7s, 1.4s, 3s, 4.4s, and 6s). Figure 11 shows the CA accuracy increases as the increment of the sliding window length and becomes stable at about 90% with four or more PPG segments. Therefore, we adopt the sliding window with 4 continuous PPG segments in our system, which not only provides the high CA accuracy but also has the short response time for the authentication (i.e., around 3s).

Impact of Training Data Size. Since the training data size influences the ease of use in terms of the time for data collection, so we particularly test 1, 2, 3, 4, 5, and 6 mins' static PPG signals of each user for training respectively, and use the rest data for testing. Figure 12(a) shows that an average CA accuracy of 77.75% is achieved only using 1 min's data of each user for training. Moreover, the average CA accuracy can increase to 90.65% and becomes stable when using 5-mins or more training data of each user. Those results prove that our system is suitable for practical use since it can achieve very high CA accuracy with the only limited size of training data (e.g., 5-mins per user).

Impact of Machine Learning Methods. We study the performance of our system with different underlying machine learning models. Specifically, we adopt the support vector machine (SVM) and neural network (NN) using the LIBSVM library [45] and the multi-layer perceptron in Scikit-learn [46], respectively. Figure 12(b) shows that GBT has the best CA accuracy of 90% compared with SVM (scaling the data) and NN whose CA accuracy is 75% and 80% respectively. This result indicates that GBT easily tuned with flexible optimization options is more suitable for our CA system than the machine learning methods which either are difficult to determine the appropriate kernel (e.g., SVM) or require a large amount of training data and expertise to tune the model (e.g., NN).

Impact of Sampling Rate. The sampling rate affects the power consumption and computational cost in the wearable devices. In particular, we find that the CA accuracy is as high as 88% at the lowest sampling rate (i.e., $25Hz$) and increases slightly with the increased sampling rate and becomes stable with 90.7% CA accuracy since $100Hz$. Those findings imply that our CA system is not only compatible with the commodity wrist-worn wearable devices (e.g., Samsung Simband [47] adopts $128Hz$ PPG sampling rate) but also supports the hardware with even lower PPG sampling rate.

E. CA Performance with MA Mitigation and MA Removal

We next study the performance of our MA removal method on near-wrist activities and MA mitigation method on far-wrist activities among 5 participants, respectively. As shown in Figure 13, while performing far-wrist activities such as moving forearm, our system could still achieve 72.2% CA accuracy even without applying the MA mitigation method and the CA accuracy increases to 89.2% after MA mitigation. Furthermore, we can see that our system has the CA accuracy as 36.6% before MA removal and achieve 75.2% after MA removal for the near-wrist activities such as grabbing up a cup to mimic drinking water gesture. Those results show that the far-wrist activities have a relatively slight impact on our CA system, whereas the near-wrist activities have more impacts due to the involvement of the tendon and muscle in the wrist area. Overall, our system has a decent performance after applying the MA mitigation method on the far-wrist activities and the MA removal method on the near-wrist activities, which implies that it's practical when the sparse and mild movements occur.

F. CA Performance with Continuous Motion Artifacts Mitigation

We study the performance of our MA mitigation method on 7 continuous motion artifacts among 4 participants, respectively. As shown in Figure 14, our system achieves an average CA accuracy of 69% and 74% under 7 continuous movements after adopting the VMD-based and CEEMDAN-based MA mitigation, respectively. Compared to the performance without any mitigation, our system improves the CA accuracy by around 39%. Moreover, it is observable that VMD outperforms CEEMDAN in *forearm half-cycle*. The reason is that *forearm half-cycle* movement generates more high-frequency noises than other movements and VMD has better performance than CEEMDAN in term of the high-frequency noise mitigation. Overall, our system has a decent performance after continuous motion artifacts mitigation, which implies that it's practical for daily life usage.

We also study the impacts of different lengths of the sliding window on the mitigation performance. As discussed in Section V-C, there exist the minimum and maximum window length constraints for continuous PPG MAs mitigation. Therefore, a *short window* (i.e., 12 seconds corresponds to the minimum requirement) and a *long window* (i.e., 24 seconds

This article has been accepted for publication in a future issue of this journal, but has not been fully edited. Content may change prior to final publication. Citation information: DOI 10.1109/JIOT.2021.3128290, IEEE Internet of Things Journal

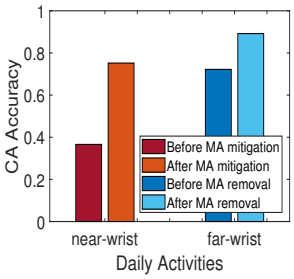

Fig. 13: Performance of MA mitigation and removal with transient activities.

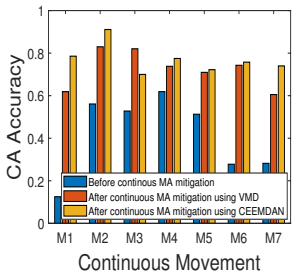

Fig. 14: Performance with mitigating 7 continuous movements (i.e.,M1 to M7).

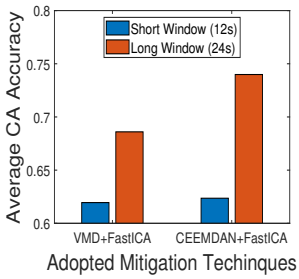

Fig. 15: Performance comparison with different lengths of the sliding windows.

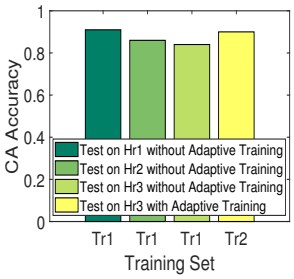

Fig. 16: Performance comparison with adaptive training.

corresponds to the maximum length constraint) are especially evaluated. Figure 15 shows that, when adopting the *short window*, both VMD + FastICA and CEEMDAN + FastICA have similar performance (i.e., 62% and 63% CA accuracy, respectively). After using the *long window*, their CA accuracies reach to 69% and 74% (increase 7% and 11%, respectively). This result demonstrates that an appropriate longer sliding window could indeed lead to better performance.

G. Effectiveness of Adaptive Training

We evaluate our adaptive training using the data collected by one user across three different hours in a day. Specifically, we collect 1-hour PPG data starting at 11 AM, 1 PM, and 4 PM, respectively. In Figure 16, $Tr1$ represents the training set is only from the first hour and Tr_2 represents the mixed training set includes the data from both the first hour and 2 mins' data from the third hour. We can see that our system trained by $Tr1$ can achieve 91% CA accuracy during the first hour, and decreases 5% during the second hour and 7% during the third hour, respectively. These results demonstrate that the user cardiac system indeed has some fluctuations during a long-time period that slightly impact the CA performance. Moreover, after the adaptive retraining with Tr_2, the CA accuracy will increase back to 90% during the third hour. Those results prove that our system is suitable for long-time user authentication with few times of adaptively retraining which requires a very small amount of the new data. (e.g., routinely retrain every 3 hours with only 2 mins' new data).

VIII. Discussion

Human Emotion Impact. We are aware that cardiac patterns may be affected by human emotions [48] with different degrees. Particularly, the emotions with high arousal (e.g., angry) may cause drastic cardiac status changes and impact the performance of our system. it is worth noting that unexpected sickness could have comparable impacts. In those cases, our system would notify the users of using the traditional authentication approach (e.g., password) to verify their identity temporarily, then update itself using the adaptive learning afterward.

PPG Sensor Impact. The light sources of the PPG sensor have different impacts on the quality of the PPG measurements. Specifically, three types of light sources (i.e., green, red, and infrared) are known to be adopted by the PPG sensor in the commodity smartwatches (e.g., Apple Watch Series 4, 5, and 6). Those lights can penetrate the human skin and tissues with different depths due to their different wavelengths. The green light is the most popular PPG light source that has the shallowest skin penetration and is hence more resistant to motion artifacts. Skin tone, specifically the amount of melanin, affects the skin's ability to absorb green light and further increases the variation in signal quality. Combining green light with red and/or infrared light sources has the potential to achieve better performance for our system. The reason is two-fold: First, red and infrared light can reach deeper tissues to capture more user-specific physiological information. Second, they are transparent to melanin and hence not appreciably affected by the skin color, tattoos, freckle patterns.

Energy Consumption. Our wearable prototype includes an Arduino board (i.e., about 50mA) and one PPG sensor (i.e., 4mA). In total, it is about 54mA current consumption of this prototype. Given the fact that the off-the-shelf smartwatches generally have a battery capacity of 380mAh, our system can run up to 7 hours on the wearable prototype. For our commodity smartwatch prototype, if we offload the computation to a smartphone via Bluetooth, the power consumption of the smartwatch [49] only involves the PPG sensor and Bluetooth (i.e., 3.5mA), which is as low as 7.5mA. Given such low power consumption, our system can run over 24 hours on a smartwatch.

IX. Conclusion

In this paper, we develop a low-cost PPG-based continuous user authentication (CA) system, TrueHeart, using the wrist-worn wearable devices. Specifically, we explore the diverse PPG measurements among 20 participants and determine the representative and general fiducial feature sets that can facilitate our CA system. We develop an effective motion artifact (MA) detection method based on the statistics of the PPG segments. In addition, MA classification and the adaptive MA filtering approaches are designed to mitigate the impacts of the transient activities and continuous activities from the daily life. To ensure the long-term robustness of our CA system, we develop an adaptive user authentication method using the gradient boosting tree (GBT) technique. We devise a wrist-worn PPG sensing prototype and a smartwatch prototype to conduct extensive experiments with 20 participants under static and different moving scenarios. The results show that our system can achieve a high average CA accuracy of over

90% and a low attack false detection rate of 4% under static scenarios in practice. Our adaptive MA mitigation approaches can improve the CA accuracy by around 39% under both transient and continuous daily activity scenarios.

ACKNOWLEDGMENT

This work was partially supported by the National Science Foundation Grants CNS1566455, CNS1826647, CNS1954959, CNS1820624, CCF2000480, CCF2028873, CCF1909963, CCF2028876, CCF2028858, ECCS2033433 and ARO Grant W911NF-18-1-0221.

REFERENCES

[1] A. H. Lashkari, S. Farmand, D. Zakaria, O. Bin, D. Saleh *et al.*, "Shoulder surfing attack in graphical password authentication," *arXiv preprint arXiv:0912.0951*, 2009.

[2] A. J. Aviv, K. L. Gibson, E. Mossop, M. Blaze, and J. M. Smith, "Smudge attacks on smartphone touch screens." *Woot*, vol. 10, pp. 1–7, 2010.

[3] A. Bhargav-Spantzel, A. C. Squicciarini, S. Modi, M. Young, E. Bertino, and S. J. Elliott, "Privacy preserving multi-factor authentication with biometrics," *Journal of Computer Security*, vol. 15, no. 5, pp. 529–560, 2007.

[4] A. Ometov, S. Bezzateev, N. Mäkitalo, S. Andreev, T. Mikkonen, and Y. Koucheryavy, "Multi-factor authentication: A survey," *Cryptography*, vol. 2, no. 1, p. 1, 2018.

[5] A. Al Abdulwahid, N. Clarke, I. Stengel, S. Furnell, and C. Reich, "A survey of continuous and transparent multibiometric authentication systems," in *European Conf. on Cyber Warfare and Security*, 2015, pp. 1–10.

[6] I. Traore, I. Woungang, M. S. Obaidat, Y. Nakkabi, and I. Lai, "Combining mouse and keystroke dynamics biometrics for risk-based authentication in web environments," in *Proceedings of the Fourth International Conference on Digital Home Digital Home (IEEE ICDH)*, 2012, pp. 138–145.

[7] S. Mare, A. M. Markham, C. Cornelius, R. Peterson, and D. Kotz, "Zebra: Zero-effort bilateral recurring authentication," in *Security and Privacy (SP), 2014 IEEE Symposium on*. IEEE, 2014, pp. 705–720.

[8] Y. Ren, Y. Chen, M. C. Chuah, and J. Yang, "User verification leveraging gait recognition for smartphone enabled mobile healthcare systems," *IEEE Transactions on Mobile Computing*, vol. 14, no. 9, pp. 1961–1974, 2015.

[9] J. Yu, L. Lu, Y. Chen, Y. Zhu, and L. Kong, "An indirect eavesdropping attack of keystrokes on touch screen through acoustic sensing," *IEEE Transactions on Mobile Computing*, 2019.

[10] S. J. Kang, S. Y. Lee, H. I. Cho, and H. Park, "Ecg authentication system design based on signal analysis in mobile and wearable devices," *IEEE Signal Processing Letters*, vol. 23, no. 6, pp. 805–808, 2016.

[11] J. R. Pinto, J. S. Cardoso, A. Lourenço, and C. Carreiras, "Towards a continuous biometric system based on ecg signals acquired on the steering wheel," *Sensors*, vol. 17, no. 10, p. 2228, 2017.

[12] F. Lin, C. Song, Y. Zhuang, W. Xu, C. Li, and K. Ren, "Cardiac scan: A non-contact and continuous heart-based user authentication system," in *Proceedings of the 23rd Annual International Conference on Mobile Computing and Networking (ACM MobiCom)*, 2017, pp. 315–328.

[13] A. Bonissi, R. D. Labati, L. Perico, R. Sassi, F. Scotti, and L. Sparagino, "A preliminary study on continuous authentication methods for photoplethysmographic biometrics," in *Biometric Measurements and Systems for Security and Medical Applications (BIOMS), 2013 IEEE Workshop on*. IEEE, 2013, pp. 28–33.

[14] A. Sarkar, A. L. Abbott, and Z. Doerzaph, "Biometric authentication using photoplethysmography signals," in *Biometrics Theory, Applications and Systems (BTAS), 2016 IEEE 8th International Conference on*. IEEE, 2016, pp. 1–7.

[15] N. Karimian, M. Tehranipoor, and D. Forte, "Non-fiducial ppg-based authentication for healthcare application," in *Proceedings of the 2017 IEEE EMBS International Conference on Biomedical & Health Informatics (BHI)(IEEE EMBS)*, 2017, pp. 429–432.

[16] N. Karimian, Z. Guo, M. Tehranipoor, and D. Forte, "Human recognition from photoplethysmography (ppg) based on non-fiducial features," in *Proceedings of the 2017 IEEE International Conference on Acoustics, Speech and Signal Processing (IEEE ICASSP)*, 2017, pp. 4636–4640.

[17] M. A. S. Mondol, I. A. Emi, S. M. Preum, and J. A. Stankovic, "User authentication using wrist mounted inertial sensors," in *Proceedings of the 16th ACM/IEEE International Conference on Information Processing in Sensor Networks*, 2017, pp. 309–310.

[18] P. Casale, O. Pujol, and P. Radeva, "Personalization and user verification in wearable systems using biometric walking patterns," *Personal and Ubiquitous Computing*, vol. 16, no. 5, pp. 563–580, 2012.

[19] A. Rahman, V. Lubecke, O. Boric-Lubecke, J. Prins, and T. Sakamoto, "Doppler radar techniques for accurate respiration charac-terization and subject identification," *IEEE Journal on Emerging and Selected Topics in Circuits and Systems*, 2018.

[20] M. Guennoun, N. Abbad, J. Talom, S. M. M. Rahman, and K. El-Khatib, "Continuous authentication by electrocardiogram data," in *Proceedings of the 2009 IEEE Toronto International Conference Science and Technology for Humanity (IEEE TIC-STH)*, 2009, pp. 40–42.

[21] C. Camara, P. Peris-Lopez, L. Gonzalez-Manzano, and J. Tapiador, "Real-time electrocardiogram streams for continuous authentication," *Applied Soft Computing*, vol. 68, pp. 784–794, 2018.

[22] X. Niu, H. Han, S. Shan, and X. Chen, "Continuous heart rate measurement from face: a robust rppg approach with distribution learning," in *2017 IEEE International Joint Conference on Biometrics (IJCB)*. IEEE, 2017, pp. 642–650.

[23] J. T. Shepherd and P. M. Vanhoutte, "The human cardiovascular system. facts and concepts," 1979.

[24] A. R. Kavsaoğlu, K. Polat, and M. R. Bozkurt, "A novel feature ranking algorithm for biometric recognition with ppg signals," *Computers in biology and medicine*, vol. 49, pp. 1–14, 2014.

[25] M. Elgendi, "On the analysis of fingertip photoplethysmogram signals," *Current cardiology reviews*, vol. 8, no. 1, pp. 14–25, 2012.

[26] T. Hastie, R. Tibshirani, and J. Friedman, "The elements of statistical learning new york," *NY: Springer*, 2009.

[27] C. Becker, R. Rigamonti, V. Lepetit, and P. Fua, "Supervised feature learning for curvilinear structure segmentation," in *International Conference on Medical Image Computing and Computer-Assisted Intervention*. Springer, 2013, pp. 526–533.

[28] M. Galar, A. Fernández, E. Barrenechea, H. Bustince, and F. Herrera, "An overview of ensemble methods for binary classifiers in multi-class problems: Experimental study on one-vs-one and one-vs-all schemes," *Pattern Recognition*, vol. 44, no. 8, pp. 1761–1776, 2011.

[29] L. Pu, P. J. Chacon, H.-C. Wu, and J.-W. Choi, "Novel tailoring algorithm for abrupt motion artifact removal in photoplethysmogram signals," *Biomedical Engineering Letters*, vol. 7, no. 4, pp. 299–304, 2017.

[30] T. Zhao, Y. Wang, J. Liu, Y. Chen, J. Cheng, and J. Yu, "Trueheart: Continuous authentication on wrist-worn wearables using ppg-based biometrics," in *IEEE INFOCOM 2020-IEEE Conference on Computer Communications*. IEEE, 2020, pp. 30–39.

[31] E. K. Antonsson and R. W. Mann, "The frequency content of gait," *Journal of biomechanics*, vol. 18, no. 1, pp. 39–47, 1985.

[32] S. Sadeghi, H. Behnam, and J. Tavakkoli, "Ultrasound elastography using empirical mode decomposition analysis," *Journal of medical signals and sensors*, vol. 4, no. 1, p. 18, 2014.

[33] A. Stallone, A. Cicone, and M. Materassi, "New insights and best practices for the successful use of empirical mode decomposition, iterative filtering and derived algorithms," *Scientific reports*, vol. 10, no. 1, pp. 1–15, 2020.

[34] M. B. Mashhadi, M. Farhadi, M. Essalat, and F. Marvasti, "Low complexity heart rate measurement from wearable wrist-type photoplethysmographic sensors robust to motion artifacts," in *2018 IEEE International Conference on Acoustics, Speech and Signal Processing (ICASSP)*. IEEE, 2018, pp. 921–924.

[35] W. He, Y. Ye, Y. Li, H. Xu, L. Lu, W. Huang, and M. Sun, "Variational mode decomposition-based heart rate estimation using wrist-type photoplethysmography during physical exercise," in *2018 24th International Conference on Pattern Recognition (ICPR)*. IEEE, 2018, pp. 3766–3771.

[36] S. Hadiyoso, E. Dewi, and I. Wijayanto, "Comparison of emd, vmd and eemd methods in respiration wave extraction based on ppg waves," in *Journal of Physics: Conference Series*, vol. 1577, no. 1. IOP Publishing, 2020, p. 012040.

[37] S. Wu, F. Feng, J. Zhu, C. Wu, and G. Zhang, "A method for determining intrinsic mode function number in variational mode decomposition and its application to bearing vibration signal processing," *Shock and Vibration*, vol. 2020, 2020.

[38] M. A. Colominas, G. Schlotthauer, and M. E. Torres, "Improved complete ensemble emd: A suitable tool for biomedical signal processing," *Biomedical Signal Processing and Control*, vol. 14, pp. 19–29, 2014.

[39] A. Hyvarinen, "Fast and robust fixed-point algorithms for independent component analysis," *IEEE transactions on Neural Networks*, vol. 10, no. 3, pp. 626–634, 1999.
[40] M. Müller, "Dynamic time warping," *Information retrieval for music and motion*, pp. 69–84, 2007.
[41] L. F. A. Martinez, J. R. Atencia, and J. Širokỳ, "Multilead beat detector based on independent component analysis (ica)."
[42] J. Sanchez, M. Ortigueira, R. Rato, and J. Trujillo, "An improved empirical mode decomposition for long signals," *SIGNAL 2016 Editors*, p. 65, 2016.
[43] T. Bombardini, V. Gemignani, E. Bianchini, L. Venneri, C. Petersen, E. Pasanisi, L. Pratali, D. Alonso-Rodriguez, M. Pianelli, F. Faita *et al.*, "Diastolic time–frequency relation in the stress echo lab: filling timing and flow at different heart rates," *Cardiovascular ultrasound*, vol. 6, no. 1, p. 15, 2008.
[44] W. Karlen, S. Raman, J. M. Ansermino, and G. A. Dumont, "Multiparameter respiratory rate estimation from the photoplethysmogram," *IEEE Transactions on Biomedical Engineering*, vol. 60, no. 7, pp. 1946–1953, 2013.
[45] C.-C. Chang and C.-J. Lin, "LIBSVM: A library for support vector machines," *ACM Transactions on Intelligent Systems and Technology*, vol. 2, pp. 27:1–27:27, 2011, software available at http://www.csie.ntu.edu.tw/ cjlin/libsvm.
[46] F. Pedregosa, G. Varoquaux, A. Gramfort, V. Michel, B. Thirion, O. Grisel, M. Blondel, P. Prettenhofer, R. Weiss, V. Dubourg, J. Vanderplas, A. Passos, D. Cournapeau, M. Brucher, M. Perrot, and E. Duchesnay, "Scikit-learn: Machine learning in Python," *Journal of Machine Learning Research*, vol. 12, pp. 2825–2830, 2011.
[47] Simband. (2017) Why is 128 hz used as a sampling frequency for the ppg signals? [Online]. Available: http://www.simband.io/documentation/faq.html
[48] M. S. Lee, Y. K. Lee, D. S. Pae, M. T. Lim, D. W. Kim, and T. K. Kang, "Fast emotion recognition based on single pulse ppg signal with convolutional neural network," *Applied Sciences*, vol. 9, no. 16, p. 3355, 2019.
[49] X. Liu, T. Chen, F. Qian, Z. Guo, F. X. Lin, X. Wang, and K. Chen, "Characterizing smartwatch usage in the wild," in *Proceedings of the 15th Annual International Conference on Mobile Systems, Applications, and Services*. ACM, 2017, pp. 385–398.

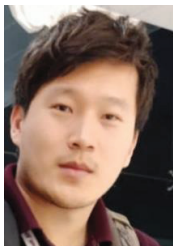

Tianming Zhao received his B.E. from the Department of Software Engineering, Chongqing University, China and his M.S. degrees from the Department of computer science, Binghamton University, USA. Currently, he is a Ph.D. student of the Computer & Information Sciences Department at Temple University. His research interests include mobile computing and sensing, cyber security and privacy, and smart health. He is currently working with Prof. Yan Wang.

Yan Wang is an Assistant Professor with Computer & Information Sciences Department at Temple University. Before that, he was with Department of Computer Science at SUNY, Binghamton. He received his Ph.D. degree in Electrical Engineering from Stevens Institute of Technology. His research interests include Cyber Security and Privacy, Internet of Things, Mobile and Pervasive Computing, and Smart Healthcare. His research is supported by the National Science Foundation (NSF). He is the recipient of the Best Paper Award from IEEE CNS 2018, IEEE SECON 2017 and ACM AsiaCCS 2016. He is the Winner of ACM MobiCom Student Research Competition, 2013. His research has been reported in numerous media outlets including MIT Technology Review, CNN, Fox News Channel, Wall Street Journal, National Public Radio, and IEEE Spectrum.

Jian Liu is an Assistant Professor in the Department of Electrical Engineering and Computer Science at the University of Tennessee, Knoxville. He received his Ph.D. degree in Wireless Information Network Laboratory (WINLAB) at Rutgers University. His current research interests include mobile sensing and computing, cybersecurity and privacy, intelligent systems and machine learning. He is the recipient of the Best Paper Awards from IEEE SECON 2017 and IEEE CNS 2018. He also received Best-in-session Presentation Award from IEEE INFOCOM 2017, and two Best Poster Award Runner-up from ACM MobiCom 2016 and 2018.

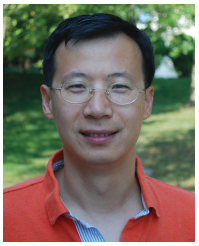

Jerry Cheng is an Assistant Professor of Computer Science at New York Institute of Technology. His research interests include big data analytics, statistical learning, Bayesian statistics, and their applications in computer systems and smart healthcare. He was an Assistant Professor in Robert Wood Johnson Medical School at Rutgers University. He was formerly a Postdoc Researcher in the Department of Statistics at Columbia University and had extensive industrial experiences as a Member of Technical Staff at AT&T Labs. His background is a combination of Computer Science, Statistics and Physics. His work has been reported by many new media including MIT Technology Review, Yahoo News, Digital World, FierceHealthcare, and WTOP Radio.

Yingying (Jennifer) Chen is a Professor of Electrical and Computer Engineering and Peter Cherasia Endowed Faculty Scholar at Rutgers University. She is the Associate Director of Wireless Information Network Laboratory (WINLAB). She also leads the Data Analysis and Information Security (DAISY) Lab. She is an IEEE Fellow. Her research interests include mobile sensing and computing, cyber security and privacy, Internet of Things, and smart healthcare. Her background is a combination of Computer Science, Computer Engineering and Physics. She had extensive industry experiences at Nokia previously. She has published over 200 journal articles and conference papers. She is the recipient of multiple Best Paper Awards from EAI HealthyIoT 2019, IEEE CNS 2018, IEEE SECON 2017, ACM AsiaCCS 2016, IEEE CNS 2014 and ACM MobiCom 2011. She is also the recipient of NSF CAREER Award and Google Faculty Research Award. She received NJ Inventors Hall of Fame Innovator Award and is also the recipient of IEEE Region 1 Technological Innovation in Academic Award. Her research has been reported in numerous media outlets including MIT Technology Review, CNN, Fox News Channel, Wall Street Journal, National Public Radio and IEEE Spectrum. She has been serving/served on the editorial boards of IEEE Transactions on Mobile Computing (IEEE TMC), IEEE Transactions on Wireless Communications (IEEE TWireless), IEEE/ACM Transactions on Networking (IEEE/ACM ToN) and ACM Transactions on Privacy and Security.

Jiadi Yu is currently an Associate Professor in Department of Computer Science and Engineering, Shanghai Jiao Tong University, Shanghai, China. Prior to join Shanghai Jiao Tong University, he was at Stevens Institute of Technology, USA as a Postdoc. Dr. Yu received the PhD degree in computer science from Shanghai Jiao Tong University, China, in 2007. Dr. Yu has published more than 100 refereed papers in international leading journals and key conferences in the areas of wireless communications and networking, mobile computing, and security & privacy. His current research interests include mobile computing and sensing, cyber security and privacy, Internet of Things (IoT), smart healthcare. He is a member of the IEEE and the IEEE Communication Society.